Research

New Phytologist

Reduced global plant respiration due to the acclimation of leaf dark respiration coupled with photosynthesis

Yanghang Ren[1], Han Wang[1], Sandy P. Harrison[1,2], I. Colin Prentice[1,3], Owen K. Atkin[4,5], Nicholas G. Smith[6], Giulia Mengoli[3], Artur Stefanski[7] and Peter B. Reich[7,8,9]

[1]Department of Earth System Science, Ministry of Education Key Laboratory for Earth System Modeling, Institute for Global Change Studies, Tsinghua University, Beijing, 100084, China; [2]School of Archaeology, Geography and Environmental Sciences (SAGES), University of Reading, Reading, RG6 6AH, UK; [3]Department of Life Sciences, Georgina Mace Centre for the Living Planet, Imperial College London, Silwood Park Campus, Buckhurst Road, Ascot, SL5 7PY, UK; [4]ARC Centre of Excellence in Plant Energy Biology, Research School of Biology, The Australian National University, Building 134, Canberra, ACT, 2601, Australia; [5]Division of Plant Sciences, Research School of Biology, The Australian National University, Building 46, Canberra, ACT, 2601, Australia; [6]Department of Biological Sciences, Texas Tech University, Lubbock, TX 79409, USA; [7]Department of Forest Resources, University of Minnesota, St Paul, MN 55108, USA; [8]Institute for Global Change Biology, and School for the Environment and Sustainability, University of Michigan, Ann Arbor, MI 48109, USA; [9]Hawkesbury Institute for the Environment, Western Sydney University, Penrith, NSW, 2753, Australia

Author for correspondence:
Han Wang
Email: wang_han@tsinghua.edu.cn

Received: *2 February 2023*
Accepted: *10 October 2023*

New Phytologist (2024) **241:** 578–591
doi: 10.1111/nph.19355

Key words: carboxylation capacity, climate change, dark respiration, eco-evolutionary optimality, global carbon cycle, land surface model, plant acclimation.

Summary

- Leaf dark respiration (R_d) acclimates to environmental changes. However, the magnitude, controls and time scales of acclimation remain unclear and are inconsistently treated in ecosystem models.
- We hypothesized that R_d and Rubisco carboxylation capacity (V_{cmax}) at 25°C ($R_{d,25}$, $V_{cmax,25}$) are coordinated so that $R_{d,25}$ variations support $V_{cmax,25}$ at a level allowing full light use, with $V_{cmax,25}$ reflecting daytime conditions (for photosynthesis), and $R_{d,25}/V_{cmax,25}$ reflecting night-time conditions (for starch degradation and sucrose export). We tested this hypothesis temporally using a 5-yr warming experiment, and spatially using an extensive field-measurement data set. We compared the results to three published alternatives: $R_{d,25}$ declines linearly with daily average prior temperature; R_d at average prior night temperatures tends towards a constant value; and $R_{d,25}/V_{cmax,25}$ is constant.
- Our hypothesis accounted for more variation in observed $R_{d,25}$ over time ($R^2 = 0.74$) and space ($R^2 = 0.68$) than the alternatives. Night-time temperature dominated the seasonal time-course of R_d, with an apparent response time scale of *c.* 2 wk. V_{cmax} dominated the spatial patterns.
- Our acclimation hypothesis results in a smaller increase in global R_d in response to rising CO_2 and warming than is projected by the two of three alternative hypotheses, and by current models.

Introduction

About a quarter of the carbon taken up globally through photosynthesis is released to the atmosphere via respiration from plant leaves (Campioli *et al.*, 2016; Huntingford *et al.*, 2017; Wang *et al.*, 2020). This flux is three times larger than anthropogenic CO_2 emissions from fossil fuel burning (Friedlingstein *et al.*, 2022) and is one of the key targets for model predictions of the global carbon cycle. Leaf respiration occurs both in the dark and in the light, but temperature-normalized rates are typically lower in the light (Tcherkez *et al.*, 2017), and leaf respiration is most commonly measured in darkness (dark respiration, R_d), either during the night, or in dark-adjusted leaves during the day. As an enzyme-catalysed process, R_d increases near-exponentially with warming on a time scale of minutes to hours (Heskel *et al.*, 2016). This instantaneous response, if sustained, would contribute to a positive feedback between the global carbon cycle and climate warming (He *et al.*, 2018; Collalti *et al.*, 2020). However, R_d acclimates to environmental changes on time scales from days (Atkin *et al.*, 2000; Bolstad *et al.*, 2003; Lee *et al.*, 2005) to weeks (Reich *et al.*, 2016) by down- or upregulation of the basal respiration rate, which is the value of R_d adjusted to a standard reference temperature, often 25°C ($R_{d,25}$; Atkin & Tjoelker, 2003; Smith & Dukes, 2013; Crous *et al.*, 2022). Thermal acclimation of $R_{d,25}$ – a lowering of the basal rate under prolonged warming – is observed in response to both experimental warming (Drake *et al.*, 2016; Reich *et al.*, 2016) and temporal changes in growth temperature (Atkin *et al.*, 2000; Lee *et al.*, 2005). The response of $R_{d,25}$ to environmental conditions is also manifested by spatial variation across sites, reflecting a combination of inherent differences between species, species replacement along environmental gradients, and acclimation by

the species present (e.g. Atkin *et al.*, 2015; Wang *et al.*, 2020; Zhu *et al.*, 2021).

Downregulation of $R_{d,25}$ with warming is expected to reduce the positive carbon-climate feedback (Ballantyne *et al.*, 2017; relative to the hypothetical case where such downregulation does not occur). However, there is no accepted, quantitative theory to predict the acclimation of $R_{d,25}$ in response to environmental change (Vanderwel *et al.*, 2015). Many land surface models (LSMs) still neglect temporal acclimation of $R_{d,25}$ and also oversimplify spatial patterns by assuming a fixed $R_{d,25}$ for each of a limited number of plant functional types (PFTs; Crous *et al.*, 2022).

Three hypotheses have been advanced to explain the temporal and/or spatial regulation of $R_{d,25}$. The first (H1) is that $R_{d,25}$ acclimates to the daily (24 h) average temperature (T_{daily}) during the past few days (Atkin *et al.*, 2015), declining linearly with increasing T_{daily} according to an empirical function. Some LSMs (e.g. JULES, CABLE, ELM) implement temporal acclimation via H1 (Huntingford *et al.*, 2017; Haverd *et al.*, 2018; Zhu *et al.*, 2019; Butler *et al.*, 2021). They assign empirical, PFT-specific parameter values (leaf nitrogen content and the rate of thermal acclimation), thereby introducing additional uncertainties (Smith & Dukes, 2013; Lombardozzi *et al.*, 2015; Collalti *et al.*, 2020).

The second (H2) and third (H3) hypotheses represent different expressions of the coupling between R_d and photosynthetic capacity (expressed as the maximum rate of Rubisco carboxylation, V_{cmax}). H2 proposes that $R_{d,25}$ acclimates to prior temperatures during the night, keeping night-time R_d not quite constant but within a modest window of variation (Reich *et al.*, 2016, 2021). H2 implicitly expresses the coupling between R_d and V_{cmax}, as higher V_{cmax} would result in higher respiratory ATP demand during the night (related to T_{night}) for the greater degradation and export of photosynthetic products (Stitt & Schulze, 1994; Turnbull *et al.*, 2002), while failure of this process would lead to feedback inhibition of V_{cmax} (Lee *et al.*, 2005; Tcherkez *et al.*, 2017; Crous *et al.*, 2022). Based on repeated observations from a long-term warming experiment in Minnesota (B4WarmED: Boreal Forest Warming at an Ecotone in Danger experiment), Reich *et al.* (2016, 2021) showed that seasonal and climate change-induced variations in $R_{d,25}$ were indeed consistent with an acclimatory response to antecedent average night-time temperatures (T_{night}) and more so than to antecedent T_{daily}. Field experiments on wheat have also shown that respiration acclimates to antecedent T_{night} (Posch *et al.*, 2021).

H3 proposes instead (although the ideas are more complementary than exclusive) that $R_{d,25}$ tends to maintain a fixed ratio to $V_{cmax,25}$ (Wang *et al.*, 2020), as assumed in the standard model of photosynthesis (Farquhar *et al.*, 1980). H3 can be motivated by the fact that V_{cmax} depends on the maintenance of Rubisco and other Calvin cycle enzymes via ATP-dependent protein synthesis in the light (Berry *et al.*, 1986). Rubisco constitutes a substantial fraction (about a half) of total leaf protein (Spreitzer & Salvucci, 2002; Di Stefano *et al.*, 2018), and a significant part of the energy supplied by R_d in mature leaves is used to support protein turnover. H3 thus implies that R_d reflects a requirement to maintain a given amount of Rubisco (Wang *et al.*, 2020). Moreover, according to the 'coordination hypothesis', long-term average V_{cmax} tends towards an optimum ($V_{cmax,opt}$), whereby the Rubisco-limited photosynthetic rate equals the electron-transport limited rate (Chen *et al.*, 1993; Haxeltine & Prentice, 1996; Maire *et al.*, 2012), which in turn depends on light. V_{cmax} appears to be related most closely to midday conditions, allowing plants to make use of all the available light (Yamori *et al.*, 2006; Mengoli *et al.*, 2022). Wang *et al.* (2020) applied H3, together with the coordination hypothesis, to explain spatial patterns in R_d. They showed that H3 predicted the observed relationship between $R_{d,25}$ and prevailing growth temperature among sites in different climates.

H2 and H3 both link R_d with V_{cmax}: H3 explicitly and H2 implicitly because: higher V_{cmax} likely results in higher rates of CO_2 fixation, greater starch accumulation and greater rates of starch degradation and sucrose export at night, resulting in higher respiratory ATP demand; and failure to process the products of photosynthesis would quickly lead to inhibition of V_{cmax}. H3 on the contrary disregards the role of T_{night} in regulating $R_{d,25}$ as shown, for example, by Reich *et al.* (2021).

V_{cmax} is related to leaf nitrogen (N) concentration, considered as a controlling variable in H1. Higher N concentrations are associated with greater demand for respiratory energy for protein turnover (Reich *et al.*, 2008; Tjoelker *et al.*, 2008; Rogers, 2014). However, as a significant amount (*c.* 20–60%) of leaf N is structural (Lamport, 1966; Onoda *et al.*, 2004; Takashima *et al.*, 2004), there is not a unique relationship between leaf N and metabolic activity (Dong *et al.*, 2017, 2022). H2 and H3 may therefore both be considered closer to the underlying physiological processes than H1.

Here, we propose a fourth hypothesis (H4) that combines aspects of H2 and H3. We hypothesize that $R_{d,25}$ acclimates to night-time temperature, in such a way as to support $V_{cmax,25}$ at a level which, in turn, acclimates to daytime meteorological conditions following the coordination hypothesis. Thus, we allow seasonal and spatial variation in $V_{cmax,25}$ to influence the respiratory demand, while assuming that this demand is mainly satisfied by respiration at night. That is, R_d acclimates to environmental changes both at night (for starch degradation and sucrose export) and during the day (for the regeneration of Rubisco), so as to provide just the right amount of ATP to support an optimal V_{cmax}.

The time scale of R_d acclimation is a separate question that applies equally to all hypotheses. Early experimental studies indicated that acclimation occurs within a few days of exposure to temperature changes (Atkin *et al.*, 2000; Bolstad *et al.*, 2003; Lee *et al.*, 2005). Applications of H1 have assumed that $R_{d,25}$ acclimates to T_{daily} at a time scale of 10 d (Huntingford *et al.*, 2017; Butler *et al.*, 2021). These studies did not test what averaging period for prior temperatures best-predicted observations. Based on analysis of data from B4WarmED, Reich *et al.* (2021) found that acclimation (following H2) was best explained (in terms of goodness of fit to observations) by somewhat longer prior time periods. Gymnosperms showed two peaks at 5–10 and 40–60 nights; angiosperms showed a single broad peak at 30–60 nights.

Assuming a mechanistic linkage between R_d and V_{cmax}, an acclimation time scale of 1–2 wk is plausible, given that the acclimation of V_{cmax} to the environment is achieved by regulating the amount of Rubisco in the leaf and the half-life of Rubisco is *c.* 1 wk (Simpson *et al.*, 1981; Yamori *et al.*, 2006; Atkin *et al.*, 2008). This time scale is further supported by measurements on *Pinus sylvestris* over a full growing season, showing acclimation of V_{cmax} on a time scale of 14 d (Mäkelä *et al.*, 2008); and by a recent modelling study, showing that observed diurnal cycles of gross primary production based on eddy-covariance flux measurements were best predicted when the time scale of V_{cmax} acclimation was set at 15 d (Mengoli *et al.*, 2022).

In this study, we compared the predictive power of the four alternative hypotheses, with a principal focus on H4, considering both acclimation through the growing season in the B4WarmED experiment and geographic patterns in a large data set spanning a range of climates. We also tested the timescales of acclimation, by comparing the goodness of fit achieved at different averaging periods. Finally, we quantified the impact of including a realistic treatment of R_d acclimation on the global carbon cycle, by comparing estimates of the annual global carbon release via acclimated leaf respiration predicted by four hypotheses over the past two decades to LSM-derived estimates in which the long-term response of R_d in the field is (unrealistically) equated to its instantaneous response, as measured, for example by Heskel *et al.* (2016) and others.

Materials and Methods

Respiratory acclimation hypotheses

Key features of H1–H4, as implemented here, are summarized in Table 1 and Supporting Information Fig. S1. H1 states that the acclimation of $R_{d,25}$ is driven by leaf nitrogen content ($n_{1,a}$) and the average daily mean temperature (T_{daily}) over the past 10 d (Huntingford *et al.*, 2017). Plant functional type-specific parameters (i.e. r_0, r_1, r_2 and $n_{1,a}$) were estimated from Atkin *et al.* (2017).

H2 states that $R_{d,25}$ acclimates to the average night-time mean temperature (T_{night}) during an averaging period of 3–60 nights. This implies a tendency towards a constant value of R_d evaluated at the acclimated temperature ($R_{d,accl}$). There is little difference between $R_{d,accl}$ values fitted using control or warming samples (0.48 and 0.43 CO_2 m^{-2} s^{-1} respectively). Therefore, we estimated $R_{d,accl}$ as 0.45 μmol CO_2 m^{-2} s^{-1}, the mean value of all field measurements including the control and warming samplings in the B4WarmED experiment (Reich *et al.*, 2021). We applied the empirical equation from Heskel *et al.* (2016) to evaluate R_d at acclimated temperatures (T_{accl}):

$$R_{d,accl} = R_{d,25} \times f_r(T_{accl}) \quad \text{Eqn 1}$$

$$f_r(T_{accl}) = \exp\left[0.1012(T_{accl}-25)-0.0005\left(T_{accl}^2-25^2\right)\right] \quad \text{Eqn 2}$$

H3 states that $R_{d,25}$ tends to maintain a constant ratio to an optimal value of $V_{cmax,25}$. We estimate this ratio as 0.03, the mean value of all field measurements in Wang *et al.* (2020).

Optimal $V_{cmax,25}$ at the whole-canopy scale was then predicted by the big-leaf framework in two steps. First, $V_{cmax,opt}$ was assumed to acclimate to average midday environmental conditions (temperature, pressure, atmosphere CO_2 concentration, vapour pressure deficit (VPD), and the light absorbed by the leaves (I_{abs})) during the prior 15 d (Mengoli *et al.*, 2022) and was predicted from the coordination hypothesis (Wang *et al.*, 2017a; Smith *et al.*, 2019a; Jiang *et al.*, 2020; Mengoli *et al.*, 2022; Fig. S2) as follows:

$$V_{cmax,opt} = \phi_0 I_{abs}[(c_i+K)/(c_i+2\Gamma^*)]\sqrt{\left\{1-\left[c^*\frac{(c_i+2\Gamma^*)}{(c_i-\Gamma^*)}\right]^{2/3}\right\}} \quad \text{Eqn 3}$$

where φ_0 is the intrinsic quantum efficiency of photosynthesis (mol mol^{-1}) derived from an empirical temperature-dependent function fitted to experimental data by Bernacchi *et al.* (2003). I_{abs} is the light absorbed by the leaves (μmol m^{-2} s^{-1}), which is the product of the fraction of absorbed photosynthetically active radiation (f_{PAR}) and incident solar radiation (W m^{-2}) with a conversion factor of 2.04 μmol J^{-1} (Meek *et al.*, 1984). K is the effective Michaelis–Menten coefficient of Rubisco (Pa), and Γ* is the photorespiratory compensation point (Pa). Both K and Γ* are temperature-dependent. c^* is a cost factor for electron-transport

Table 1 Four respiratory acclimation hypotheses.

Hypotheses	Equations	Factors controlling $R_{d,25}$	Acclimation time scale	Empirical parameters	References
H1	$R_{d,25} = r_0 + r_1 n_{1,a} - r_2 T_{daily}$	Daily average temperature (T_{daily}), leaf nitrogen content ($n_{1,a}$)	10 d	PFT-specific r_0, r_1, r_2 and $n_{1,a}$	Huntingford *et al.* (2017)
H2	$R_{d,25} = R_{d,accl}/f_r(T_{night})$	Night-time average temperature (T_{night})	1–90 d	$R_{d,accl}$ = 0.45 μmol CO_2 m^{-2} s^{-1}	Reich *et al.* (2021)
H3	$R_{d,25} = b_{25} V_{cmax,25}$	Maximum capacity of carboxylation at 25°C ($V_{cmax,25}$)	15 d	b_{25} = 0.03	Wang *et al.* (2020)
H4	$R_{d,25} = b\frac{f_v(T_{day})}{f_r(T_{night})} V_{cmax,25}$	$V_{cmax,25}$, T_{night}, daytime temperature (T_{day})	1–90 d	b = 0.018	This study

$R_{d,25}$ represents the value of R_d (dark leaf respiration) adjusted to a 25°C. $R_{d,accl}$ indicates the value of R_d evaluated at the acclimated temperature. f_r is the temperature response of R_d (Heskel *et al.*, 2016), while f_v is the Arrhenius equation.

capacity, estimated as 0.41 (Wang *et al.*, 2017a). c_i is the leaf-internal CO_2 partial pressure (Pa), estimated by the least-cost hypothesis as a function of ambient partial pressure of CO_2, temperature, atmospheric pressure and VPD (Wang *et al.*, 2017a,b). The functions for determining φ_0, K, Γ^* and c_i are all described in Fig. S2. All climatic variables were calculated as daytime averages over the past 15 d except for the instantaneous VPD (in order to account for the fast response of stomata to VPD). For C_4 plants, $V_{cmax,opt}$ was predicted by assuming both $(c_i + K)/(c_i + 2\Gamma^*)$ and $(c_i + 2\Gamma^*)/(c_i - \Gamma^*)$ to be close to unity (Scott & Smith, 2022), with φ_0 estimated following Cai & Prentice (2020).

Second, we estimated $V_{cmax,opt}$ at 25°C by inverting the Arrhenius equation:

$$V_{cmax,25} = V_{cmax,opt} \times f_v^{-1}(T_{accl}) \quad \text{Eqn 4}$$

$$f_v(T_{accl}) = \exp\left[(\Delta H_a/R)\frac{T_{accl}-25}{298.15(T_{accl}+273.15)}\right] \quad \text{Eqn 5}$$

where ΔH_a is the activation energy of V_{cmax} (65 330 J mol^{-1}, Bernacchi *et al.*, 2001). R is the universal gas constant (8.314 J mol^{-1} K^{-1}) and T_{accl} is the average midday temperature over the past 15 d. We considered using more complex, peaked functions (Kumarathunge *et al.*, 2019, coloured curves in Fig. S3) instead of the Arrhenius equation, but the added complexity made almost no difference (Fig. S3) – due to the fact that most of the observations (B4WarmED, GlobResp and leaf carbon exchange (LCE)) fell to the left-hand side of the peak.

H4 states that $R_{d,accl}$ is proportional to $V_{cmax,opt}$. We estimated the proportionality factor as 0.018 based on the combined dataset (see the details in the next section). Similar to H2, $R_{d,accl}$ can be represented as a product of $R_{d,25}$ and a function of T_{accl} (Eqns 1, 2), which is taken to be T_{night} averaged over the prior nights. $V_{cmax,opt}$ can also be represented as product of $V_{cmax,25}$ and a function of T_{accl} (Eqns 4, 5), where T_{accl} is given by prior daytime temperatures averaged over the same period as T_{night}.

Unlike the explicit acclimation time scale for H1 (10 d) and H3 (15 d), the predictions of H2 and H4 were assessed based on their best performance over averaging periods ranging from 1 to 90 d. The four hypotheses were then evaluated by comparing their predictions with the observations.

Respiration and climate data

We used three $R_{d,25}$ datasets (Fig. S4): B4WarmED (Reich *et al.*, 2021), the Global Leaf Respiration Database (GlobResp: Atkin *et al.*, 2015) and (LCE: Smith & Dukes, 2017, 2018) data set (Table S1). B4WarmED includes multi-year (2009–2013) measurements of R_d from 10 species grown at ambient temperature and at 3.4°C above ambient temperature. B4WarmED also records the prior night-time (when the sun elevation was $< 0°$, i.e. below the horizon), daytime (9:00–15:00 h), 24 h temperatures and 24 h VPD, averaged (across all 30-min averages) for the prior 1–90 d (or nights) at the site level, which are used to drive the predictions. (Daytime here is defined differently from Mengoli *et al.*, 2022, who used the average of 11:30, 12:00 and 12:30 to represent midday. The difference is however relatively small compared with the spatial and temporal variation in daytime temperature.)

We combined GlobResp and LCE to create a spatial data set. GlobResp provides measured $R_{d,25}$ for 899 species at 100 sites world-wide. We determined the exact sampling dates from published papers and field documents to extract the prior environmental conditions for each sample from a global forcing dataset. LCE contains R_d field measurements with known sampling dates of 98 species from sites in North and Central America spanning 53° of latitude.

All three datasets followed a similar measurement protocol: Fully expanded leaves were taken in the morning and were measured in a darkened chamber after at least 10 min dark adjustment. GlobResp provides $R_{d,25}$ directly; LCE and B4WarmED provided measured leaf temperature, so instantaneous R_d ($R_{d,ins}$) at the measured temperature (T_{ins}) could be adjusted to the standard 25°C according to $R_{d,ins} = R_{d,25} \bullet f_r$ (T_{ins}) (Heskel *et al.*, 2016). After excluding samples for which no measurement date was recorded, the dataset compiled from B4WarmED, GlobResp and LCE provided a total of > 3500 $R_{d,25}$ samples from 2006 to 2016 covering 53 sites (Table S1). Most of the samples were from C_3 plants, but there were 121 samples from C_4 plants. The compiled dataset also provides measured V_{cmax}; thus, we used this combined dataset to derive the factor b in H4 (0.018) as the mean ratio of measured R_d and V_{cmax}. The term $R_{d,accl}$ in H2 was estimated (0.45 μmol CO_2 m^{-2} s^{-1}) as the mean R_d of all field measurements from B4WarmED. The term b_{25} in H3 was estimated (0.03) based on the combined LCE and GlobResp dataset using the mean ratio of measured $R_{d,25}$ and $V_{cmax,25}$. $R_{d,25}$ at the canopy level predicted by H3 and H4 was downscaled by leaf area index (LAI) to the average-canopy $R_{d,25}$ for further comparison with the observations, because the field sampling involved collecting leaves developed at a range of irradiances at different levels in the canopy. From the top to the bottom of the canopy, H3 and H4 predict that leaf-level $R_{d,25}$ decreases along with $V_{cmax,25}$ in accordance with light exposure, following Beer's law as shown in Fig. S5.

The environmental inputs needed to predict $R_{d,25}$ for each sample in the spatial data sets, and to simulate global leaf respiration, were obtained from global gridded datasets. The WATCH Forcing Data Methodology applied to ERA5 (WFDE5) includes global bias-corrected meteorological variables, with a spatial resolution of 0.5°, hourly from 1979 to 2019 (Cucchi *et al.*, 2020). Here, we selected the WFDE5 air temperature, air pressure, specific humidity and solar radiation as the meteorological variables and averaged the hourly data to daytime, night-time and 24 h values for the prior 1 to 90 d (or nights). Vapour pressure deficit was calculated based on air temperature and specific humidity following Buck (1981). Global monthly atmospheric CO_2 concentration was obtained from the National Oceanic and Atmospheric Administration (NOAA; Ballantyne *et al.*, 2012). To eliminate the effect of clouds, LAI from the reprocessed MODIS LAI v.6 product (Yuan *et al.*, 2011) was used to estimate f_{PAR} from Beer's law with $k = 0.5$ (Dong *et al.*, 2017). The

reprocessed version provides a global 8-d LAI at 0.5° from 2001 to 2020, which was linearly interpolated to yield daily LAI. For the prediction of $R_{d,25}$ for individual samples, we used location and sampling date to extract the appropriate environmental inputs before the sampling date. For the global simulation, we used gridded forcings at 0.5° resolution from 2001 to 2019.

Data analysis

Statistical analysis focused on testing the factors controlling R_d acclimation and identifying the time scale of R_d acclimation at the species and community levels. For B4WarmED, the community level was the average of all repeated samples within 1 d of the year (DOY, hereafter 'doy-mean'). The variations of doy-mean $R_{d,25}$ represent temporal acclimation to seasonal environmental changes. For the dataset created by combining GlobResp and LCE, the community level was the average of all samples at a given site (hereafter 'site-mean'). Site-mean $R_{d,25}$ includes the combined effects of species selection and acclimation across climatic gradients.

The predictions of H2 and H4 were assessed based on their best performance over averaging periods ranging from 1 to 90 d. We then calculated the predictive ability (R^2) and root mean square error (RMSE) of each hypothesis driven by differing factors compared with the observed $R_{d,25}$, both temporally (in B4WarmED) and spatially (in GlobResp + LCE). After evaluating the performance of each of these hypotheses, we calculated the R^2 and RMSE between observations and predictions of the hypothesis with best performance among the four hypotheses using averaging periods of 1–90 d for the predictions. We identified the acclimation time scale as the period yielding the lowest RMSE. Although the maximum R^2 has been used to identify the time scale of acclimation, for example by Reich *et al.* (2021), we found that R^2 tends to plateau with increasing time-window width irrespective of the true time scale of acclimation when the dependent and independent variables are nonlinearly related (see details in Fig. S6). The longer timescales indicated by the maximum R^2 are likely caused by smoothing over a longer time interval, which reduces random variation. Unlike R^2, RMSE here shows a clear minimum – and thus provides a more robust indication of the acclimation time scale (Fig. S6).

We used bisquare-weighted robust regression (Imhoff *et al.*, 2007; Zacksenhouse *et al.*, 2009) since this reduces the effect of outliers on the regression results by assigning smaller weights to outliers. We used the ROBUSTFIT package in MATLAB to perform regressions of $R_{d,25}$ observation and prediction, which returned the weighted RMSE. The weighted R^2 was calculated as:

$$R^2 = 1 - \frac{\sum_{i=1}^{i=n}\left[w_i\left(y_i - f_i\right)^2\right]}{\sum_{i=1}^{i=n}\left[w_i\left(y_i - \bar{y}\right)^2\right]} \quad \text{Eqn 6}$$

where the w_i are the weightings (from 0 to 1) for each data point i, the y_i are the observed values, the f_i are the predicted values, and $\bar{y}$ is the mean observed value.

Global impact of acclimation

We compared global leaf respiration from 2001 to 2019 in simulations with acclimation (Case 0) and without acclimation (Case 1). For Case 0, acclimation was incorporated using each of the four acclimation hypotheses. Comparison between the Case 0 simulations allows us to explore the effects of different approaches to acclimation. For the Case 1 simulations, we adopted the PFT-specific $R_{d,25}$ parameters from four LSMs: NOAH-MP (Niu *et al.*, 2011), JULES (Clark *et al.*, 2011), CLM4.0 (Bonan & Levis, 2010) and ORCHIDEE (Krinner *et al.*, 2005). Although each of the four LSMs treats $R_{d,25}$ as a PFT-specific parameter, they parameterize $R_{d,25}$ differently. We therefore assessed the impact of acclimation by comparing the Case 0 simulations to the ensemble mean of the four LSMs to reduce the uncertainty due to dependence on a single model formulation. NOAH-MP provides parameter values of $R_{d,25}$ for each PFT in a look-up table; the other three LSMs use leaf age and nitrogen content to calculate $R_{d,25}$ for each PFT. PFT-$R_{d,25}$ for these three models were derived from the PFT-specific $V_{cmax,25}$ using the coefficients of proportionality 0.015 (C_3 plants) and 0.025 (C_4 plants) (Collatz *et al.*, 1991; Clark *et al.*, 2011), which has the same meaning as the term b_{25} in H3 (see Table. 1). This simplification is acceptable here because we are concerned with the temporal trend in global R_d rather than its absolute magnitude. To compare the temporal changes in R_d more clearly, we rescaled the R_d simulated by different schemes using R_d in 2001 from H4 as the base value. Driven by the same inputs, the difference in the temporal changes in R_d simulated by Case 0 and Case 1 indicates the impacts of acclimation on global leaf respiration.

Results

Factors controlling the acclimation of leaf respiration

T_{night} and V_{cmax} together best explained the temporal variations of $R_{d,25}$, which was predominantly controlled by T_{night} (Fig. 1a–d). The two hypotheses that accounted for the effect of T_{night}, H2 and H4, explained the variability of doy-mean $R_{d,25}$ derived from B4WarmED consistently better than H3, which considered only the effect of $V_{cmax,25}$, or H1, which considered the effects of N_{leaf} and T_{daily} (Fig. 1a–d). H4 had slightly greater explanatory power overall ($R^2 = 0.31$) than H2 ($R^2 = 0.29$; Fig. 1b,d), but species varied in this respect (Fig. S7). Half of the species showed >10 percentage point improvements in R^2 under H4 as compared to H2. Consistent with the pattern shown by R^2, RMSE of seven species showed > 0.02 μmol CO_2 m^{-2} s^{-1} improvement under H4 compared with H2.

H4, combining the effects of T_{night} and V_{cmax}, best captured the magnitude of the temporal variations of $R_{d,25}$. The observed doy-mean $R_{d,25}$ varied from 0.57 to 2.17 μmol CO_2 m^{-2} s^{-1}. H1 displayed the smallest changes among the four hypotheses (Fig. 1a–d), with estimated doy-mean $R_{d,25}$ varying more narrowly (between 1.11 and 1.64 μmol CO_2 m^{-2} s^{-1}), and a general overestimation. Compared with H1, H3 better demonstrated the

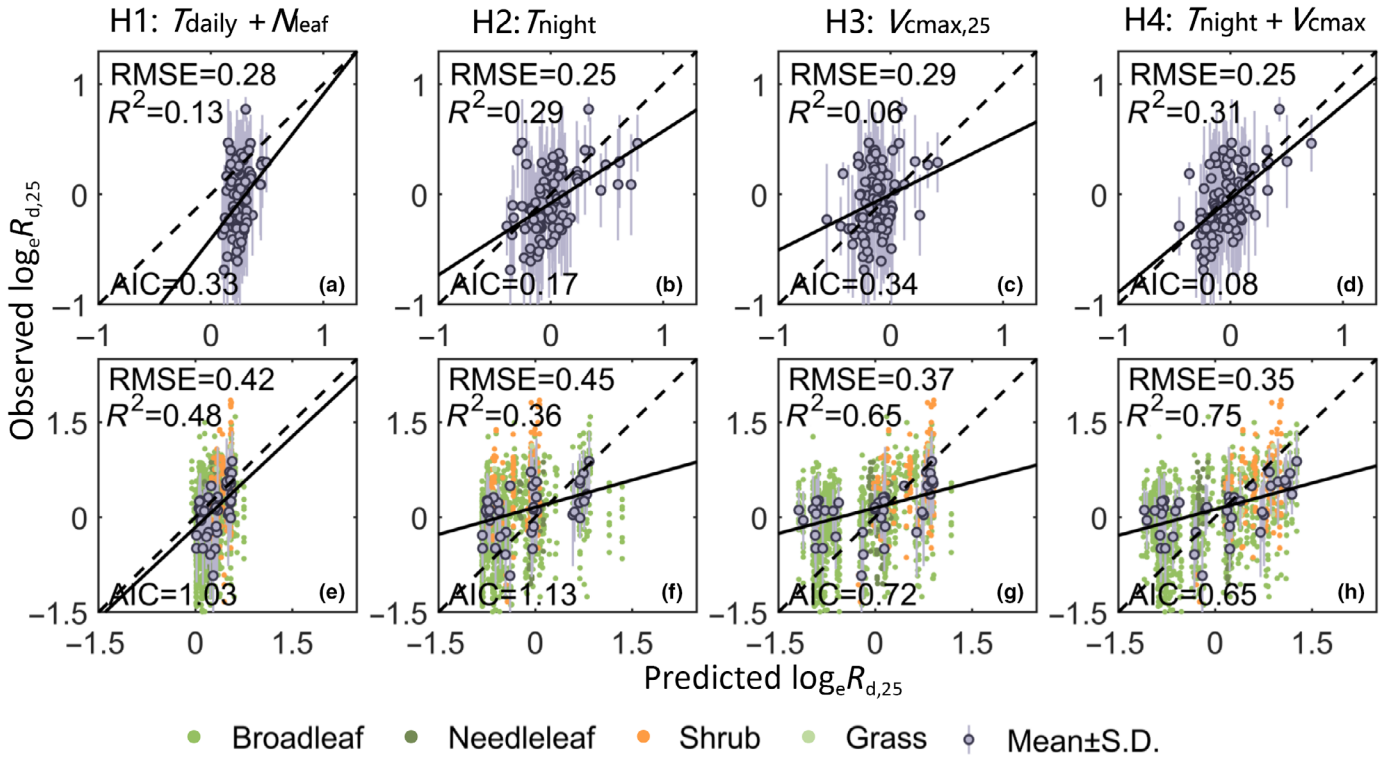

Fig. 1 Scatter plots of natural-log transformed $R_{d,25}$ between observations and predictions according to the four hypotheses using their best-performing acclimation timescales for H2 and H4 while fixed acclimation time scales for H1 and H3 (10 and 15 d, respectively). The controlling factors are daily averaged temperature (T_{daily}), leaf nitrogen content (N_{leaf}), night-time averaged temperature (T_{night}) and maximum capacity of carboxylation at 25°C ($V_{cmax,25}$). The temporal observations are from the B4WarmED dataset (a–d) and the spatial observations are from the combined GlobResp and leaf carbon exchange (LCE) datasets (e–h). Mean values are the average of all species within the sampling day (doy_mean, a–d) or site (site_mean, e–h), respectively. S.D. means the standard deviation. The solid black line is the fitted line of the robust regression, and the dashed line represents the 1 : 1 line. R^2 and root mean square error (RMSE) are the weighted coefficient of determination and weighted root mean square error between observed and predicted $R_{d,25}$. AIC is the Akaike information criterion, which quantifies the performance of alternative hypotheses after accounting for the different degrees of freedom. All statistical analyses are based on the doy_mean values (a–d) or site site_mean values (e, f).

variation in smaller respiration rates, but underestimated larger respiration rates with estimated doy-mean $R_{d,25}$ varying from 0.57 to 1.52 μmol CO_2 m^{-2} s^{-1}. The ranges of variation in doy-mean $R_{d,25}$ under H2 and H4, from 0.68 to 2.19 μmol CO_2 m^{-2} s^{-1} and from 0.63 to 2.06 μmol CO_2 m^{-2} s^{-1}, respectively, were broadly consistent with the observed range, while the line fitted under H4 was closer to 1 : 1.

Geographic variation in observed site-mean $R_{d,25}$ (Fig. 1e–h) was also best explained by the combined effects of T_{night} and V_{cmax} ($R^2 = 0.75$). The relatively good fit of H3 ($R^2 = 0.65$) indicated that this was primarily the result of variability in $V_{cmax,25}$. However, the improvement (by 10 percentage points) in R^2 from H3 to H4 implies that additional pattern was captured by the consideration of T_{night} as well as $V_{cmax,25}$. T_{daily} and N_{leaf} (H1; $R^2 = 0.48$) and T_{night} alone (H2; $R^2 = 0.36$), represented the geographic variation of $R_{d,25}$ less well than H3 or H4.

Accounting for the degrees of freedom, the importance of T_{night} and V_{cmax} for $R_{d,25}$ was further supported by AIC (Akaike information criterion), which was smallest for H4 (Fig. 1). Compared with the results mixing both factors and timescales (Fig. 1), the comparisons using the fixed time window (e.g. 15 d) between four hypotheses (Fig. S8) also showed that H4 had the best performance, providing solid evidence for the importance of both T_{night} and V_{cmax} in regulating $R_{d,25}$.

Time scales of acclimation

The best prediction (lowest RMSE) for temporal variations in $R_{d,25}$, considering all species together, under H4 was obtained for the 15-d averaging period (Fig. 2a). The median RMSE of observed $R_{d,25}$ and predicted $R_{d,25}$ declined from 0.43 to 0.15 μmol CO_2 m^{-2} s^{-1} for B4WarmED (Fig. 2a) as the averaging period was increased from 1 to 15 d. RMSE remained almost stable from 15 to 45 d, implying that acclimation might continue for longer than 15 d; but RMSE did not improve after 15 d, indicating that most acclimation was accomplished within 15 d. RMSE increased again as the time window was lengthened from 45 to 90 d.

R^2 variations were broadly consistent with the optimal time scale of acclimation indicated by the RMSE. Median R^2 for the 10 species was 0.37 at the 15-d time scale, lower than the value of 0.46 obtained at the 45-d time scale, but there was little difference in the 25th and 75th percentile of R^2 values between the 15-d and 45-d averaging periods.

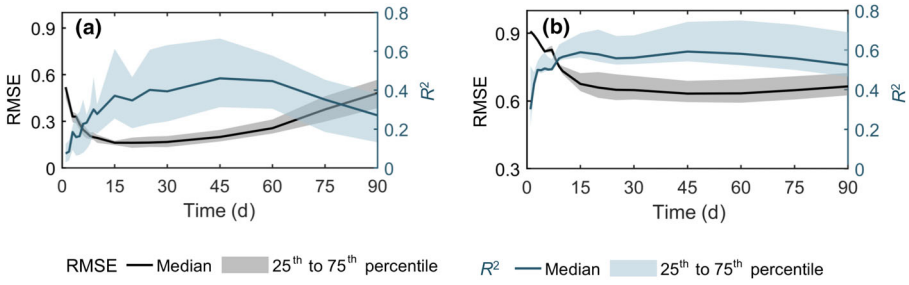

Fig. 2 Estimating the acclimation time scale of leaf respiration. The relationship (R^2 and root mean square error (RMSE)) of doy-mean $R_{d,25}$ observations to $R_{d,25}$ predictions according to H4 for different numbers of prior days, derived from (a) the B4WarmED dataset and (b) the combined GlobResp and leaf carbon exchange (LCE) dataset.

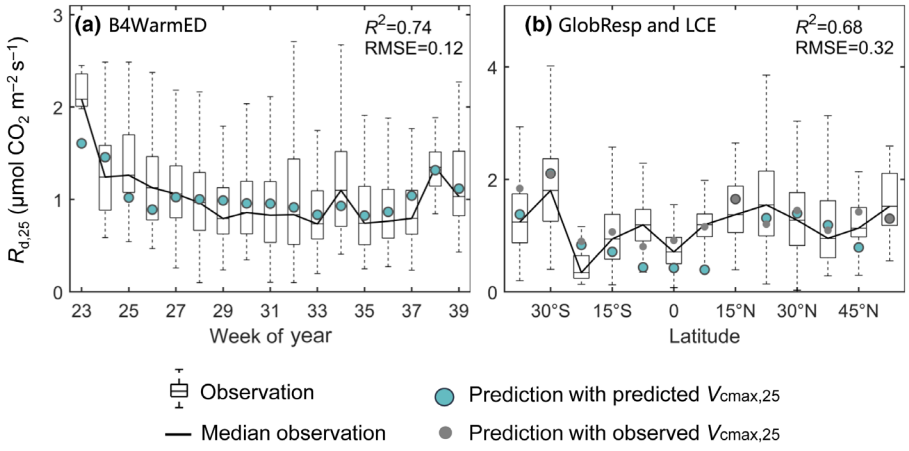

Fig. 3 Seasonal (a) and latitudinal (b) variations of $R_{d,25}$ predicted by H4 with an acclimation time scale of 15 d. The boxplot indicates the observed $R_{d,25}$ (25th percentile, 75th percentile and median; maximum and minimum for the whiskers) (a) weekly averaged for 2009–2013 or (b) site-averaged in the 7.5° latitudinal bands. The black curves show the variations of observed median $R_{d,25}$. The points are the predicted $R_{d,25}$ using predicted $V_{cmax,25}$ (blue points) and observed $V_{cmax,25}$ (grey points) as H4's inputs, respectively. R^2 and root mean square error (RMSE) are based on the predicted $R_{d,25}$ using our predicted $V_{cmax,25}$. LCE, leaf carbon exchange.

Supported by the measurements from the combined GlobResp and LCE datasets (Fig. 2b), the 15-d averaging period emerges as the best according to the RMSE criterion, as well as being consistent with physiological expectations. Derived from the spatial analysis, the median RMSE for four PFTs declined from 0.91 to 0.67 μmol CO_2 m^{-2} s^{-1} as the averaging period was increased from 1 to 15 d, while the median R^2 stabilized after 15 d. But as this analysis was based on single measurements at each site (rather than repeated measurements over a season), it reflects a combination of species replacement along environmental gradients and acclimation by the species present and provides weaker evidence for the time scale, and cannot meaningfully distinguish among the longer time scales.

H4 with an acclimation time scale of 15 d captured both the observed seasonal cycle and latitudinal trend in $R_{d,25}$ derived from B4WarmED dataset and from the combined GlobResp and LCE dataset, respectively (Fig. 3). The multi-year weekly mean observation in $R_{d,25}$ for all species showed some seasonal pattern, with highest $R_{d,25}$ at the beginning and end of the growing season. The median predictions in $R_{d,25}$ for different weeks were close to the median observations, with an RMSE of 0.16 μmol CO_2 m^{-2} s^{-1} and an R^2 of 0.74. The model also predicted the median $R_{d,25}$ in different latitudinal bins reasonably well ($R^2 = 0.68$), although it underpredicted values in the equatorial band (7.5°N to 7.5°S, Fig. 3b). This underestimation was likely related to the predicted $V_{cmax,25}$ in our hypothesis, and it was improved after using observed $V_{cmax,25}$ as the input of H4. H1 yielded unrealistically muted variations of $R_{d,25}$ in both time and space ($R^2 = 0.34$ and 0.27, respectively; Fig. S9a1,b1). H2 performed well for temporal patterns only, while H3 performed well for spatial patterns only (Fig. S9a2,a3, b2,b3).

The impact of acclimation on global leaf respiration

Global simulations using H4 showed readily interpretable spatial patterns. Average-canopy $R_{d,25}$ was larger at high latitudes than in the equatorial zone (Fig. 4a), while whole-canopy R_d decreased from the equator towards the poles (Fig. 4b). Plants in tropical regions tended to minimize their $R_{d,25}$, with a mean $R_{d,25}$ of 0.43 μmol CO_2 m^{-2} s^{-1}, while plants in cold regions tended to have higher $R_{d,25}$. In high-altitude regions (including the Rocky Mountains, the Andes and the Tibetan Plateau), $R_{d,25}$ was significantly higher (up to 3.82 μmol CO^2 m^{-2} s^{-1}) than in low-elevation areas at the same latitude, due to the climate conditions (low temperature and high solar radiation). After predicting $R_{d,25}$ by H4, the global carbon emission from whole-canopy leaf respiration was simulated. The simulations showed that the tropical forest regions – the Amazon, Congo Basin and SE Asian rainforests – had relatively high total leaf respiration, despite low leaf-level $R_{d,25}$. H3 produced a similar spatial distribution of whole-canopy leaf respiration to H4 (Fig. S10c), while H1 and H2 simulated higher R_d, especially in the tropics (Fig. S10a,b).

Total global leaf respiration increased from 2001 to 2019 with the most significant increase between 2001 and 2005 (Fig. 5a), according to our H4 simulation, due to the increasing LAI. The overall magnitude of change in global R_d between 2001 and 2019 was an 8% increase in 2019 compared with 2001, from

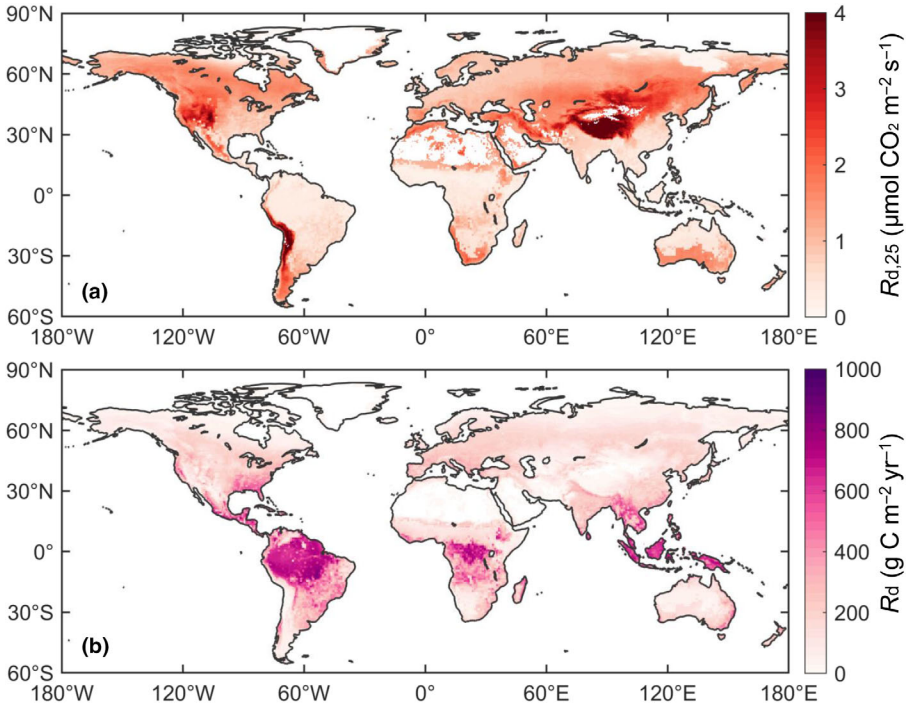

Fig. 4 Spatial patterns of (a) average-canopy $R_{d,25}$ and (b) annual whole-canopy leaf respiration from 2001 to 2019 simulated using H4. Average-canopy $R_{d,25}$ in panel (a) was simulated using the average environmental states for 2001–2019. The value of each grid was a weighted sum of the proportion of C_3 and C_4 plants. The distribution C_3 and C_4 plants was taken from Still *et al*. (2003).

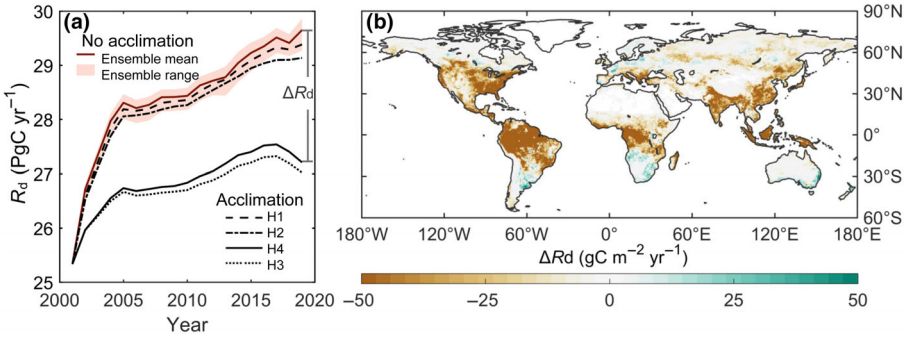

Fig. 5 Impact of acclimation on global leaf respiration from 2001 to 2019. (a) Simulated temporal changes in global total annual leaf respiration from 2001 to 2019. The black curves were simulated under the four acclimation hypotheses, H1, H2, H3 and H4. The red curve with shaded area shows the ensemble mean and range of the NOAH-MP, JULES, CLM4.0 and ORCHIDEE simulations. All predictions except H4 were rescaled based on the value of H4 in 2001. (b) The spatial distribution of the difference in R_d of H4 (solid black curve) and the ensemble mean (solid red curve) in 2019 (ΔR_d). The global total annual leaf respiration in (a) is the sum of R_d flux (unit: gC yr^{-1} per m^2) of each 0.5° grid cell multiplied by the area of the grid.

25.3 to 27.2 PgC yr^{-1}. The initial increase in global R_d was mainly caused by increased leaf biomass (indicated by LAI, see Figs S11a, S12a). The recent reduction in global R_d was driven by decreased solar radiation (Figs S11b, S12a). The generally increasing trend in global R_d was largely driven by warming and an increase in canopy biomass (Figs S11a,c, S12a), although changes in solar radiation and VPD also influenced R_d. At the global scale, the averaged response of R_d to solar radiation was largely mediated by LAI. Even though average solar radiation showed a dimming trend globally (Fig. S11b), the LAI in the brightening region was higher than that in the dimming region (Fig. S13) and therefore dominated the positive trend in the globally averaged response of R_d. Driven by the increasing LAI, the LSM simulations and other three hypotheses all showed an increasing trend in global R_d (Figs 5a, S12b).

The ensemble mean increase between 2001 and 2019 was 16% (Fig. 5a) – > 50% higher than the increase shown by H4 after accounting for acclimation of T_{night} and V_{cmax}. Decreasing $V_{cmax,25}$ primarily explains the smaller increase in R_d produced by H4 (Fig. S14a). The absolute value of the ensemble mean increase was 4.3 PgC yr^{-1}, compared with only 1.9 PgC yr^{-1} for H4. However, when using a fixed $V_{cmax,25}$ (Fig. S14a), H4 produced a large increase in R_d similar to that simulated by the LSMs. From 2001 to 2019, globally averaged $V_{cmax,25}$ continued to decrease, in response to both warming and increasing atmospheric CO_2 concentration (Fig. S14b). The increase in R_d from 2001 to 2019 according to H4 was lower over 80% of the globe (Fig. 5b) than that shown in the LSM simulations. However, H4 simulated a stronger R_d increase than the LSM simulations (i.e. positive ΔR_d) in a limited number of regions. This appears to be

caused by higher $R_{d,25}$ due to the brightening-induced increase in carboxylation capacity (Fig. S15).

Discussion

Respiratory acclimation is driven jointly by night-time temperatures and V_{cmax}

We have provided an approach to simulate both temporal and spatial variation in $R_{d,25}$ based on the hypothesis that $R_{d,25}$ is jointly controlled by prior T_{night} and V_{cmax}. Previous studies (Atkin *et al.*, 2008; Searle *et al.*, 2011; Reich *et al.*, 2021) have emphasized the importance of temperature variation on the seasonal acclimation in leaf respiration and explored whether day or night-time temperatures mattered more. Here, we have shown that predictions based on T_{daily} explained only 13% of the variability in the $R_{d,25}$ time series (Fig. 1a), compared with 29% explained by T_{night} (Fig. 1b). Bruhn *et al.* (2022) found that measurements during the day of dark-adjusted R_d would overestimate night-time R_d, due to temperature-normalized rates of the latter decreasing through the night. These results suggest that the use of T_{daily} to express R_d acclimation in models (Atkin *et al.*, 2008; Huntingford *et al.*, 2017) is not sufficient to capture the full impact of growth temperature on leaf respiration. Although the effect of V_{cmax} on $R_{d,25}$ at the local scale was relatively small (and not apparent for all species), V_{cmax} has a large spatial variability and its effect on the spatial pattern of R_d is substantial. Wang *et al.* (2020) analysed field measurements from > 100 sites globally and concluded that $R_{d,25}$ was consistent with the acclimation of optimal photosynthetic capacity, with a sensitivity of −4.4% $°C^{-1}$. Our results showed a significant contribution of $V_{cmax,25}$ to the spatial variation of $R_{d,25}$, with an R^2 of 0.65, consistent with Wang *et al.* (2020)'s findings.

Apart from the temperature effect, our hypothesis links R_d and V_{cmax} and therefore predicts other environmental impacts on R_d via V_{cmax}. In addition to the contribution of increasing atmospheric CO_2 concentration to the reduction in $V_{cmax,25}$ (Fig. S14b), warming also leads to decreasing $V_{cmax,25}$ – leading to a smaller R_d increase by H4 from 2001 to 2019. Increasing VPD is expected to have a positive impact on $R_{d,25}$, due to higher $V_{cmax,25}$ accompanying higher VPD (Smith *et al.*, 2019a). As predicted by the least-cost hypothesis, under higher VPD, plants tend to increase investment in Rubisco to compensate for the lower CO_2 supply induced by stomatal closure (Prentice *et al.*, 2014). However, relatively few studies have analysed the effect of VPD on $R_{d,25}$; and results have been inconsistent. For example, Zhu *et al.* (2021) showed that $R_{d,25}$ increased with VPD to meet the energy requirements for repair of cellular damage associated with desiccation, while Reich *et al.* (2021) showed that $R_{d,25}$ decreased with increased VPD. The difference in the response of $R_{d,25}$ to VPD might be related to the different VPD levels in the two studies: moderate VPD stress in Reich *et al.* (2021) leading to a decrease in net photosynthetic rate, reducing the respiratory substrate and depressing $R_{d,25}$; higher VPD stress in Zhu *et al.* (2021) leading to cellular damage, requiring additional respiratory energy for repair. However, the positive impact of VPD on $R_{d,25}$ due to the increasing $V_{cmax,25}$ at higher VPD, which is a consequence of our hypothesis (Fig. S14b), is consistent with the finding of Zhu *et al.* (2021). Further controlled experiments are necessary to explore the effect of VPD on R_d. Solar radiation would also influence the acclimation of leaf respiration through a similar mechanism (changing V_{cmax}) but in the opposite direction (i.e. higher radiation should lead to higher R_d as a result of increased V_{cmax}; Fig. S2).

All hypotheses accounted less well for the variations of B4WarmED samplings (Fig. 1a–d) than they did for that of GlobResp and LCE datasets (Fig. 1e–h). However, H4 captured 74% of the variations of weekly averaged $R_{d,25}$ derived from B4WarmED (Fig. 3a).

All hypotheses yielded better predictions of temporal variation in $R_{d,25}$ for gymnosperms than for angiosperms (Fig. S7). We speculate that this might reflect our use of air temperature to represent leaf temperature (to which R_d responds), as there is expected to be a larger divergence between leaf and air temperatures in broad-leaved angiosperms than in the needle-leaved gymnosperms included here. Leaf size is a key trait affecting leaf temperature (Wright *et al.*, 2017), and broad-leaved angiosperms have larger leaves with a thicker leaf boundary layer and therefore reduced sensible heat flux between leaves and air (Gates, 1968). Thus, all else equal, the larger leaves of angiosperms should experience a larger leaf-to-air temperature difference (Leigh *et al.*, 2017). A larger leaf-to-air temperature difference provides a way to reach optimal temperatures for photosynthesis quickly on cold mornings, and thus achieve a greater carbon assimilation (Michaletz *et al.*, 2016). The leaf-to-air temperature divergence may also explain why the fitted slopes of spatial $R_{d,25}$ variations are < 1 for every hypothesis (Fig.1f–h). When we excluded pairs with predicted $\log_e R_{d,25} < -0.5$, which are predominantly broad-leaved species, the slopes became closer to 1 (Fig. S16). Another possible cause of systematic bias is uncertainty in the reanalysis air temperature. WFDE5 temperature has a spatial resolution of 0.5°, which is coarse for comparisons with experimental data. This scale mismatch may have introduced some bias into the simulation results.

Identifying the acclimation time scale

We have shown that the R_d acclimation timescale is about a fortnight, which is plausible and consistent with the life-cycle of V_{cmax} from physiological expectations and multi-sites analysis (Mäkelä *et al.*, 2008; Mengoli *et al.*, 2022). The acclimation time scales of R_d estimated in previous studies were diverse, ranging from 1 to 60 d (Bolstad *et al.*, 2003; Whitehead *et al.*, 2004; Reich *et al.*, 2021). Reich *et al.* (2021) used the maximum R^2 to identify the most explanatory time window of the seasonal variation in $R_{d,25}$, and found apparent acclimation time scales for six angiosperm species ranging from 30 to 60 d (Fig. S17). However, we found a tendency for R^2 to increase towards a plateau with increasing time scale and showed that this phenomenon can be replicated in artificial data where the true time scale is known (Fig. S6). Moreover, similar to Reich *et al.* (2021), we found two peaks in R^2 between predicted and observed $R_{d,25}$ according to

H2, especially for gymnosperms (e.g. at 8 and 45 d for *Picea glauca*; Fig. S17). Searle *et al.* (2011) also found two peaks in R^2 between the basal respiration rate and temperature for two species of alpine grass, with one at 3–5 d and one at 120 d. RMSE showed a clear minimum more often than R^2 and did not identify the multiple time scales suggested by R^2 values. The RMSE-based choice of acclimation time scale generally identified a shorter time scale than that inferred from R^2 and furthermore identified a consistent time scale across different species (Fig. S17). At the community level, the performance of H4 did not improve at longer periods (e.g. 30 d), indicating that most acclimation was accomplished within 15 d (Fig. S18). Due to the stabilization of average temperatures over longer periods, longer timescales indicated by the highest R^2 probably reflect seasonality more than short-term plasticity of thermal acclimation. The extent of acclimation might differ between pre-existing and newly developed leaves (Campbell *et al.*, 2007). It would also be worth exploring whether the acclimation time scale is influenced by location, if sufficient data on temporal variation were available from different climates.

The impact of respiratory acclimation on the global carbon cycle

R_d is commonly represented in LSMs as having a steeper temperature response than photosynthesis (Krinner *et al.*, 2005; Bonan & Levis, 2010; Niu *et al.*, 2011; He *et al.*, 2018). This representation is not consistent with observations that show R_d increasing by 3.7% $°C^{-1}$, whereas the sensitivity of V_{cmax} to growth temperature is 5.5% $°C^{-1}$ (Wang *et al.*, 2020). Hypotheses (H1 and H2) that consider thermal acclimation, but ignore the effect of V_{cmax} on $R_{d,25}$, produce a similarly strong increase in global leaf respiration between 2001 and 2019 to LSMs that do not take acclimation into account (Fig. 5a). This is due to the relatively weak temperature sensitivities of $R_{d,25}$ (e.g. -0.0402 μmol CO_2 m^{-2} s^{-1} per degree Celsius in H1) and the limited temperature change over the study period (2001–2019; Fig. S19). Dong *et al.* (2022) calculated that leaf photosynthetic N should have declined by 0.27% yr^{-1} (in proportion with decreasing leaf-level acclimated V_{cmax}) from 1986 to 2016, which would also have led to reduced leaf respiration. Our results show that the thermal acclimation of R_d coupled with V_{cmax} (H3 and H4) was indeed stronger than that estimated by ignoring V_{cmax}, as suggested by Dong *et al.* (2022), demonstrating that V_{cmax} has played an important role in the acclimation of R_d. If the T_{night} warming trend continues to be faster than that of T_{day} (Davy *et al.*, 2017; Cox *et al.*, 2020), H3 (ignoring the effects of T_{night}) might overestimate the acclimation potential of leaf respiration by the end of the century.

H4 is a general hypothesis that could straightforwardly be implemented in LSMs. It does not require PFT-specific parameters, and so could provide a simpler and more robust way of representing dark respiration than the approach used in current models (Harrison *et al.*, 2021). The constant parameters assumed in H2–H4 (e.g. $R_{d,accl}$ in H2) may, however, vary among species (Fig. S20). It is worthwhile to consider how to improve the prediction of $V_{cmax,25}$ to yield more accurate R_d predictions, especially in the tropics (Fig. 3b). Further work will be required to take account of the acclimation of fine roots and stems, given their different acclimation behaviours and importance in plant respiration (Hamilton *et al.*, 2002; Smith *et al.*, 2019b), in order to provide a more comprehensive basis for understanding how leaf-level respiratory acclimation will impact the carbon cycle.

Acknowledgements

This work has been supported by the National Natural Science Foundation of China (grant nos. 32022052, 31971495 and 72140005), Project of Industry-University-Research Cooperation between Tsinghua University and China Forestry Group Corp. on Forestry Carbon Sink Development (ZLJT-THU2022110101). ICP and SPH are supported by the High-End Foreign Expert Program of the China State Administration of Foreign Expert Affairs at Tsinghua University (G2023102014). SPH also acknowledges support from the ERC-funded project GC2.0 (Global Change 2.0: Unlocking the past for a clearer future, No. 694481). ICP also acknowledges support from the ERC under the European Union's Horizon 2020 research and innovation programme (grant agreement no: 787203 REALM). This research is a contribution to the LEMONTREE (Land Ecosystem Models based On New Theory, obseRvations and ExperimEnts) project, funded through the generosity of Eric and Wendy Schmidt by recommendation of the Schmidt Futures programme. NGS acknowledges support from the US National Science Foundation (DEB-2045968). PBR and AS acknowledge support from the US Department of Energy; Office of Science; and Office of Biological and Environmental Research award number DE-FG02-07ER644456; Minnesota Agricultural Experiment Station MN-42-030 and MN-42-060; College of Food, Agricultural, and Natural Resources Sciences and Wilderness Research Foundation of the University of Minnesota; and the NSF Biological Integration Institute program (NSF-DBI 2021898).

Competing interests

None declared.

Author contributions

YR, HW, SPH and ICP designed the study. YR, HW and ICP developed the acclimation model. GM advised on the implementation of acclimation for predictions. OKA, PBR, NGS and AS provided the data, advised on its use and contributed to the interpretation of predictions. YR, HW and SPH wrote the first version of the manuscript. All authors contributed to subsequent versions.

ORCID

Owen K. Atkin https://orcid.org/0000-0003-1041-5202
Sandy P. Harrison https://orcid.org/0000-0001-5687-1903

Giulia Mengoli https://orcid.org/0000-0003-1894-4942
I. Colin Prentice https://orcid.org/0000-0002-1296-6764
Peter B. Reich https://orcid.org/0000-0003-4424-662X
Yanghang Ren https://orcid.org/0009-0007-5056-6706
Nicholas G. Smith https://orcid.org/0000-0001-7048-4387
Artur Stefanski https://orcid.org/0000-0002-5412-1014
Han Wang https://orcid.org/0000-0003-2482-1818

Data availability

The WFDE5 climate dataset to simulate leaf respiration can be obtained from https://cds.climate.copernicus.eu/cdsapp#!/dataset/10.24381/cds.20d54e34?tab=overview. The atmospheric CO_2 concentration is publicly available at the National Oceanic and Atmospheric Administration (NOAA) (gml.noaa.gov/ccgg/trends/). The MODIS LAI v.6 product can be downloaded from globalchange.bnu.edu.cn/research/lai. The GlobResp dataset can be obtained from the Plant Trait Database (TRY) (https://www.try-db.org/TryWeb/Data.php). The LCE dataset is available in the supporting information of Smith & Dukes (2017). The B4WarmED dataset is from Reich *et al.* (2021).

References

Atkin OK, Atkinson LJ, Fisher RA, Campbell CD, Zaragoza-Castells J, Pitchford JW, Woodward FI, Hurry V. 2008. Using temperature-dependent changes in leaf scaling relationships to quantitatively account for thermal acclimation of respiration in a coupled global climate–vegetation model. *Global Change Biology* **14**: 2709–2726.

Atkin OK, Bahar NHA, Bloomfield KJ, Griffin KL, Heskel MA, Huntingford C, de la Torre AM, Turnbull MH. 2017. Leaf respiration in terrestrial biosphere models. In: Tcherkez G, Ghashghaie J, eds. *Plant respiration: metabolic fluxes and carbon balance*. Cham, Switzerland: Springer International, 107–142.

Atkin OK, Bloomfield KJ, Reich PB, Tjoelker MG, Asner GP, Bonal D, Bönisch G, Bradford MG, Cernusak LA, Cosio EG *et al.* 2015. Global variability in leaf respiration in relation to climate, plant functional types and leaf traits. *New Phytologist* **206**: 614–636.

Atkin OK, Holly C, Ball MC. 2000. Acclimation of snow gum (*Eucalyptus pauciflora*) leaf respiration to seasonal and dirunal variations in temperature: the immportance of changes in the capacity and temperature sensitivity of respiration. *Plant, Cell & Environment* **23**: 15–26.

Atkin OK, Tjoelker MG. 2003. Thermal acclimation and the dynamic response of plant respiration to temperature. *Trends in Plant Science* **8**: 343–351.

Ballantyne A, Smith W, Anderegg W, Kauppi P, Sarmiento J, Tans P, Shevliakova E, Pan Y, Poulter B, Anav A *et al.* 2017. Accelerating net terrestrial carbon uptake during the warming hiatus due to reduced respiration. *Nature Climate Change* **7**: 148–152.

Ballantyne AP, Alden CB, Miller JB, Tans PP, White JWC. 2012. Increase in observed net carbon dioxide uptake by land and oceans during the past 50 years. *Nature* **488**: 70–72.

Bernacchi CJ, Pimentel C, Long SP. 2003. In vivo temperature response functions of parameters required to model RuBP-limited photosynthesis. *Plant, Cell & Environment* **26**: 1419–1430.

Bernacchi CJ, Singsaas EL, Pimentel C, Portis AR Jr, Long SP. 2001. Improved temperature response functions for models of Rubisco-limited photosynthesis. *Plant, Cell & Environment* **24**: 253–259.

Berry JO, Nikolau BJ, Carr JP, Klessig DF. 1986. Translational regulation of light-induced ribulose 1,5-bisphosphate carboxylase gene expression in amaranth. *Molecular and Cellular Biology* **6**: 2347–2353.

Bolstad PV, Reich P, Lee T. 2003. Rapid temperature acclimation of leaf respiration rates in *Quercus alba* and *Quercus rubra*. *Tree Physiology* **23**: 969–976.

Bonan GB, Levis S. 2010. Quantifying carbon-nitrogen feedbacks in the Community Land Model (CLM4). *Geophysical Research Letters* **37**: L07401.

Bruhn D, Newman F, Hancock M, Povlsen P, Slot M, Sitch S, Drake J, Weedon GP, Clark DB, Pagter M *et al.* 2022. Nocturnal plant respiration is under strong non-temperature control. *Nature Communications* **13**: 5650.

Buck AL. 1981. New equations for computing vapor pressure and enhancement factor. *Journal of Applied Meteorology and Climatology* **20**: 1527–1532.

Butler EE, Wythers KR, Flores-Moreno H, Chen M, Datta A, Ricciuto DM, Atkin OK, Katge J, Thornton PE, Banerjee A *et al.* 2021. Updated respiration routines alter spatio-temporal patterns of carbon cycling in a global land surface model. *Environmental Research Letters* **16**: 104015.

Cai W, Prentice IC. 2020. Recent trends in gross primary production and their drivers: analysis and modelling at flux-site and global scales. *Environmental Research Letters* **15**: 124050.

Campbell C, Atkinson L, Zaragoza-Castells J, Lundmark M, Atkin O, Hurry V. 2007. Acclimation of photosynthesis and respiration is asynchronous in response to changes in temperature regardless of plant functional group. *New Phytologist* **176**: 375–389.

Campioli M, Malhi Y, Vicca S, Luyssaert S, Papale D, Peñuelas J, Reichstein M, Migliavacca M, Arain MA, Janssens IA. 2016. Evaluating the convergence between eddy-covariance and biometric methods for assessing carbon budgets of forests. *Nature Communications* **7**: 13717.

Chen J-L, Reynolds JF, Harley PC, Tenhunen JD. 1993. Coordination theory of leaf nitrogen distribution in a canopy. *Oecologia* **93**: 63–69.

Clark DB, Mercado LM, Sitch S, Jones CD, Gedney N, Best MJ, Pryor M, Rooney GG, Essery RLH, Blyth E *et al.* 2011. The Joint UK Land Environment Simulator (JULES), model description – Part 2: Carbon fluxes and vegetation dynamics. *Geoscitific Model Development* **4**: 701–722.

Collalti A, Ibrom A, Stockmarr A, Cescatti A, Alkama R, Fernández-Martínez M, Matteucci G, Sitch S, Friedlingstein P, Ciais P *et al.* 2020. Forest production efficiency increases with growth temperature. *Nature Communications* **11**: 5322.

Collatz GJ, Ball JT, Grivet C, Berry JA. 1991. Physiological and environmental regulation of stomatal conductance, photosynthesis and transpiration: a model that includes a laminar boundary layer. *Agricultural and Forest Meteorology* **54**: 107–136.

Cox DTC, Maclean IMD, Gardner AS, Gaston KJ. 2020. Global variation in diurnal asymmetry in temperature, cloud cover, specific humidity and precipitation and its association with leaf area index. *Global Change Biology* **26**: 7099–7111.

Crous KY, Uddling J, De Kauwe MG. 2022. Temperature responses of photosynthesis and respiration in evergreen trees from boreal to tropical latitudes. *New Phytologist* **234**: 353–374.

Cucchi M, Weedon GP, Amici A, Bellouin N, Lange S, Müller Schmied H, Hersbach H, Buontempo C. 2020. WFDE5: bias-adjusted ERA5 reanalysis data for impact studies. *Earth System Science Data* **12**: 2097–2120.

Davy R, Esau I, Chernokulsky A, Outten S, Zilitinkevich S. 2017. Diurnal asymmetry to the observed global warming. *International Journal of Climatology* **37**: 79–93.

Di Stefano E, Agyei D, Njoku EN, Udenigwe CC. 2018. Plant RuBisCo: an underutilized protein for food applications. *Journal of the American Oil Chemists' Society* **95**: 1063–1074.

Dong N, Prentice IC, Evans BJ, Caddy-Retalic S, Lowe AJ, Wright IJ. 2017. Leaf nitrogen from first principles: field evidence for adaptive variation with climate. *Biogeosciences* **14**: 481–495.

Dong N, Wright IJ, Chen JM, Luo X, Wang H, Keenan TF, Smith NG, Prentice IC. 2022. Rising CO_2 and warming reduce global canopy demand for nitrogen. *New Phytologist* **235**: 1692–1700.

Drake JE, Tjoelker MG, Aspinwall MJ, Reich PB, Barton CVM, Medlyn BE, Duursma RA. 2016. Does physiological acclimation to climate warming stabilize the ratio of canopy respiration to photosynthesis? *New Phytologist* **211**: 850–863.

Farquhar GD, von Caemmerer S, Berry JA. 1980. A biochemical model of photosynthetic CO_2 assimilation in leaves of C3 species. *Planta* **149**: 78–90.

Friedlingstein P, Jones MW, O'Sullivan M, Andrew RM, Bakker DCE, Hauck J, Le Quéré C, Peters GP, Peters W, Pongratz J *et al.* 2022. Global carbon budget 2021. *Earth System Science Data* **14**: 1917–2005.

Gates DM. 1968. Transpiration and leaf temperature. *Annual Review of Plant Physiology* **19**: 211–238.

Hamilton JG, DeLucia EH, George K, Naidu SL, Finzi AC, Schlesinger WH. 2002. Forest carbon balance under elevated CO_2. *Oecologia* **131**: 250–260.

Harrison SP, Cramer W, Franklin O, Prentice IC, Wang H, Brännström Å, de Boer H, Dieckmann U, Joshi J, Keenan TF *et al.* 2021. Eco-evolutionary optimality as a means to improve vegetation and land-surface models. *New Phytologist* **231**: 2125–2141.

Haverd V, Smith B, Nieradzik L, Briggs PR, Woodgate W, Trudinger CM, Canadell JG, Cuntz M. 2018. A new version of the CABLE land surface model (subversion revision r4601) incorporating land use and land cover change, woody vegetation demography, and a novel optimisation-based approach to plant coordination of photosynthesis. *Geoscientific Model Development* **11**: 2995–3026.

Haxeltine A, Prentice IC. 1996. A general model for the light-use efficiency of primary production. *Functional Ecology* **10**: 551–561.

He Y, Piao S, Li X, Chen A, Qin D. 2018. Global patterns of vegetation carbon use efficiency and their climate drivers deduced from MODIS satellite data and process-based models. *Agricultural and Forest Meteorology* **256-257**: 150–158.

Heskel MA, O'Sullivan OS, Reich PB, Tjoelker MG, Weerasinghe LK, Penillard A, Egerton JJG, Creek D, Bloomfield KJ, Xiang J *et al.* 2016. Convergence in the temperature response of leaf respiration across biomes and plant functional types. *Proceedings of the National Academy of Sciences, USA* **113**: 3832–3837.

Huntingford C, Atkin OK, Martinez-de la Torre A, Mercado LM, Heskel MA, Harper AB, Bloomfield KJ, O'Sullivan OS, Reich PB, Wythers KR *et al.* 2017. Implications of improved representations of plant respiration in a changing climate. *Nature Communications* **8**: 1602.

Imhoff M, Schettlinger K, Fried R, Gather U, Siebig S, Wrede C. 2007. Robust regression methods for intensive care monitoring. *Critical Care* **11**: P438.

Jiang C, Ryu Y, Wang H, Keenan TF. 2020. An optimality-based model explains seasonal variation in C_3 plant photosynthetic capacity. *Global Change Biology* **26**: 6493–6510.

Krinner G, Viovy N, de Noblet-Ducoudré N, Ogée J, Polcher J, Friedlingstein P, Ciais P, Sitch S, Prentice IC. 2005. A dynamic global vegetation model for studies of the coupled atmosphere-biosphere system. *Global Biogeochemical Cycles* **19**: GB1015.

Kumarathunge DP, Medlyn BE, Drake JE, Tjoelker MG, Aspinwall MJ, Battaglia M, Cano FJ, Carter KR, Cavaleri MA, Cernusak LA *et al.* 2019. Acclimation and adaptation components of the temperature dependence of plant photosynthesis at the global scale. *New Phytologist* **222**: 768–784.

Lamport DTA. 1966. The protein component of primary cell walls. *Advances in Botanical Research* **2**: 151–218.

Lee TD, Reich PB, Bolstad PV. 2005. Acclimation of leaf respiration to temperature is rapid and related to specific leaf area, soluble sugars and leaf nitrogen across three temperate deciduous tree species. *Functional Ecology* **19**: 640–647.

Leigh A, Sevanto S, Close JD, Nicotra AB. 2017. The influence of leaf size and shape on leaf thermal dynamics: does theory hold up under natural conditions? *Plant, Cell & Environment* **40**: 237–248.

Lombardozzi DL, Bonan GB, Smith NG, Dukes JS, Fisher RA. 2015. Temperature acclimation of photosynthesis and respiration: a key uncertainty in the carbon cycle-climate feedback. *Geophysical Research Letters* **42**: 8624–8631.

Maire V, Martre P, Kattge J, Gastal F, Esser G, Fontaine S, Soussana JF. 2012. The coordination of leaf photosynthesis links C and N fluxes in C_3 plant species. *PLoS ONE* **7**: e38345.

MÄKelÄ A, Pulkkinen M, Kolari P, Lagergren F, Berbigier P, Lindroth A, Loustau D, Nikinmaa E, Vesala T, Hari P. 2008. Developing an empirical model of stand GPP with the LUE approach: analysis of eddy covariance data at five contrasting conifer sites in Europe. *Global Change Biology* **14**: 92–108.

Meek DW, Hatfield JL, Howell TA, Idso SB, Reginato RJ. 1984. A generalized relationship between photosynthetically active radiation and solar radiation. *Agronomy Journal* **76**: 939–945.

Mengoli G, Agustí-Panareda A, Boussetta S, Harrison SP, Trotta C, Prentice IC. 2022. Ecosystem photosynthesis in land-surface models: a first-principles approach incorporating acclimation. *Journal of Advances in Modeling Earth Systems* **14**: e2021MS002767.

Michaletz ST, Weiser MD, McDowell NG, Zhou J, Kaspari M, Helliker BR, Enquist BJ. 2016. The energetic and carbon economic origins of leaf thermoregulation. *Nature Plants* **2**: 16129.

Niu G-Y, Yang Z-L, Mitchell KE, Chen F, Ek MB, Barlage M, Kumar A, Manning K, Niyogi D, Rosero E *et al.* 2011. The community Noah land surface model with multiparameterization options (Noah-MP): 1. Model description and evaluation with local-scale measurements. *Journal of Geophysical Research: Atmospheres* **116**: D12109.

Onoda Y, Hikosaka K, Hirose T. 2004. Allocation of nitrogen to cell walls decreases photosynthetic nitrogen-use efficiency. *Functional Ecology* **18**: 419–425.

Posch BC, Zhai D, Coast O, Scafaro AP, Bramley H, Reich PB, Ruan Y-L, Trethaowan R, Way DA, Atkin OK. 2021. Wheat respiratory O_2 consumption falls with night warming alongside greater respiratory CO_2 loss and reduced biomass. *Journal of Experimental Botany* **73**: 915–926.

Prentice IC, Dong N, Gleason SM, Maire V, Wright IJ. 2014. Balancing the costs of carbon gain and water transport: testing a new theoretical framework for plant functional ecology. *Ecology Letters* **17**: 82–91.

Reich PB, Sendall KM, Stefanski A, Wei X, Rich RL, Montgomery RA. 2016. Boreal and temperate trees show strong acclimation of respiration to warming. *Nature* **531**: 633–636.

Reich PB, Stefanski A, Rich RL, Sendall KM, Wei X, Zhao C, Hou J, Montgomery RA, Bermudez R. 2021. Assessing the relevant time frame for temperature acclimation of leaf dark respiration: a test with 10 boreal and temperate species. *Global Change Biology* **27**: 2945–2958.

Reich PB, Tjoelker MG, Pregitzer KS, Wright IJ, Oleksyn J, Machado J-L. 2008. Scaling of respiration to nitrogen in leaves, stems and roots of higher land plants. *Ecology Letters* **11**: 793–801.

Rogers A. 2014. The use and misuse of $V_{c,max}$ in earth system models. *Photosynthesis Research* **119**: 15–29.

Scott HG, Smith NG. 2022. A model of C_4 photosynthetic acclimation based on least-cost optimality theory suitable for Earth System Model incorporation. *Journal of Advances in Modeling Earth Systems* **14**: e2021MS002470.

Searle SY, Thomas S, Griffin KL, Horton T, Kornfeld A, Yakir D, Hurry V, Turnbull MH. 2011. Leaf respiration and alternative oxidase in field-grown alpine grasses respond to natural changes in temperature and light. *New Phytologist* **189**: 1027–1039.

Simpson E, Cooke RJ, Davies DD. 1981. Measurement of protein degradation in leaves of *Zea mays* using [3H]acetic anhydride and tritiated water. *Plant Physiology* **67**: 1214–1219.

Smith NG, Dukes JS. 2013. Plant respiration and photosynthesis in global-scale models: incorporating acclimation to temperature and CO_2. *Global Change Biology* **19**: 45–63.

Smith NG, Dukes JS. 2017. LCE: leaf carbon exchange data set for tropical, temperate, and boreal species of North and Central America. *Ecology* **98**: 2978.

Smith NG, Dukes JS. 2018. Drivers of leaf carbon exchange capacity across biomes at the continental scale. *Ecology* **99**: 1610–1620.

Smith NG, Keenan TF, Prentice IC, Wang H, Wright IJ, Niinemets U, Crous KY, Domingues TF, Guerrieri R, Ishida FY *et al.* 2019a. Global photosynthetic capacity is optimized to the environment. *Ecology Letters* **22**: 506–517.

Smith NG, Li G, Dukes JS. 2019b. Short-term thermal acclimation of dark respiration is greater in non-photosynthetic than in photosynthetic tissues. *AoB Plants* **11**: plz064.

Spreitzer RJ, Salvucci ME. 2002. RUBISCO: structure, regulatory interactions, and possibilities for a better enzyme. *Annual Review of Plant Biology* **53**: 449–475.

Still CJ, Berry JA, Collatz GJ, DeFries RS. 2003. Global distribution of C_3 and C_4 vegetation: carbon cycle implications. *Global Biogeochemical Cycles* **17**: 1006.

Stitt M, Schulze D. 1994. Does Rubisco control the rate of photosynthesis and plant growth? An exercise in molecular ecophysiology. *Plant, Cell & Environment* **17**: 465–487.

Takashima T, Hikosaka K, Hirose T. 2004. Photosynthesis or persistence: nitrogen allocation in leaves of evergreen and deciduous *Quercus* species. *Plant, Cell & Environment* **27**: 1047–1054.

Tcherkez G, Gauthier P, Buckley TN, Busch FA, Barbour MM, Bruhn D, Heskel MA, Gong XY, Crous KY, Griffin K *et al.* 2017. Leaf day respiration:

low CO_2 flux but high significance for metabolism and carbon balance. *New Phytologist* **216**: 986–1001.

Tjoelker MG, Oleksyn J, Reich PB, Żytkowiak R. 2008. Coupling of respiration, nitrogen, and sugars underlies convergent temperature acclimation in *Pinus banksiana* across wide-ranging sites and populations. *Global Change Biology* **14**: 782–797.

Turnbull MH, Murthy R, Griffin KL. 2002. The relative impacts of daytime and night-time warming on photosynthetic capacity in *Populus deltoides*. *Plant, Cell & Environment* **25**: 1729–1737.

Vanderwel MC, Slot M, Lichstein JW, Reich PB, Kattge J, Atkin OK, Bloomfield KJ, Tjoelker MG, Kitajima K. 2015. Global convergence in leaf respiration from estimates of thermal acclimation across time and space. *New Phytologist* **207**: 1026–1037.

Wang H, Atkin OK, Keenan TF, Smith NG, Wright IJ, Bloomfield KJ, Kattge J, Reich PB, Prentice IC. 2020. Acclimation of leaf respiration consistent with optimal photosynthetic capacity. *Global Change Biology* **26**: 2573–2583.

Wang H, Prentice IC, Cornwell WM, Keenan TF, Davis TW, Wright IJ, Evans BJ, Peng C. 2017a. Towards a universal model for carbon dioxide uptake by plants. *Nature Plants* **3**: 734–741.

Wang H, Prentice IC, Davis TW, Keenan TF, Wright IJ, Peng C. 2017b. Photosynthetic responses to altitude: an explanation based on optimality principles. *New Phytologist* **213**: 976–982.

Whitehead D, Griffin KL, Turnbull MH, Tissue DT, Engel VC, Brown KJ, Schuster WSF, Walcroft AS. 2004. Response of total night-time respiration to differences in total daily photosynthesis for leaves in a *Quercus rubra* L. canopy: implications for modelling canopy CO_2 exchange. *Global Change Biology* **10**: 925–938.

Wright IJ, Dong N, Maire V, Prentice IC, Westoby M, Díaz S, Gallagher RV, Jacobs BF, Kooyman R, Law EA *et al.* 2017. Global climatic drivers of leaf size. *Science* **357**: 917–921.

Yamori W, Suzuki K, Noguchi K, Nakai M, Terashima I. 2006. Effects of Rubisco kinetics and Rubisco activation state on the temperature dependence of the photosynthetic rate in spinach leaves from contrasting growth temperatures. *Plant, Cell & Environment* **29**: 1659–1670.

Yuan H, Dai Y, Xiao Z, Ji D, Shangguan W. 2011. Reprocessing the MODIS Leaf Area Index products for land surface and climate modelling. *Remote Sensing of Environment* **115**: 1171–1187.

Zacksenhouse M, Nemets S, Lebedev MA, Nicolelis MAL. 2009. Robust satisficing linear regression: performance/robustness trade-off and consistency criterion. *Mechanical Systems and Signal Processing* **23**: 1954–1964.

Zhu L, Bloomfield KJ, Asao S, Tjoelker MG, Egerton JJG, Hayes L, Weerasinghe LK, Creek D, Griffin KL, Hurry V *et al.* 2021. Acclimation of leaf respiration temperature responses across thermally contrasting biomes. *New Phytologist* **229**: 1312–1325.

Zhu Q, Riley WJ, Tang J, Collier N, Hoffman FM, Yang X, Bisht G. 2019. Representing nitrogen, phosphorus, and carbon interactions in the E3SM land model: development and global benchmarking. *Journal of Advances in Modeling Earth Systems* **11**: 2238–2258.

Supporting Information

Additional Supporting Information may be found online in the Supporting Information section at the end of the article.

Fig. S1 Flowchart of four respiratory acclimation hypotheses.

Fig. S2 Flowchart of the adjustment of leaf dark respiration (R_d) to the optimal carboxylation capacity and the past night-time temperature.

Fig. S3 Temperature responses implied by the use of a simple Arrhenius curve with fixed parameters (black curve) and Kumarathunge *et al.*'s (2019) peaked-Arrhenius curves (coloured curves) with acclimated parameters.

Fig. S4 Spatial distribution of the field-measured $R_{d,25}$ used in this study.

Fig. S5 Predicted variation of leaf $R_{d,25}$ within a LAI = 6 canopy following Beer's law.

Fig. S6 Relationship (R^2 and RMSE) of artificial y and T_e for differing numbers of prior days (time scales).

Fig. S7 Scatter plots of observed and predicted $R_{d,25}$ for 10 species derived from B4WarmED dataset using their best-performing acclimation timescales for H2 and H4 while fixed acclimation time scales for H1 and H3 (10 d and 15 d, respectively).

Fig. S8 Scatter plots of natural-log transformed $R_{d,25}$ between observations and predictions according to the four hypotheses using a fixed acclimation time scale of 15 d (nights).

Fig. S9 Seasonal (a1–a3) and latitudinal (b1–b3) variations of $R_{d,25}$ predicted by H1–H3 using the best-performing acclimation timescale for H3 while fixed acclimation time scales for H1 and H3 (10 d and 15 d, respectively).

Fig. S10 Spatial patterns of annual whole-canopy leaf respiration from 2001 to 2019 simulated by H1–H3.

Fig. S11 Temporal changes in global annual averaged leaf area index (LAI), solar radiation (Srad), temperature (T) and vapour pressure deficit (VPD) from 2001 to 2019.

Fig. S12 Temporal changes in global annual leaf respiration from 2001 to 2019 simulated by H4 and LSMs under different input scenarios.

Fig. S13 Comparison of averaged LAI in the dimming and brightening regions.

Fig. S14 Temporal changes in global annual leaf respiration and global averaged $V_{cmax,25}$ from 2001 to 2019 simulated by different input scenarios.

Fig. S15 Spatial distribution of the change in solar radiation: ΔSrad.

Fig. S16 Scatter plots of natural-log transformed $R_{d,25}$ between observations and predictions for all samples, and excluding samples expected to have a large temperature divergence according to H2–H4.

Fig. S17 Relationship (R^2 and RMSE) of observed $R_{d,25}$ to predicted $R_{d,25}$ according to H2 and H4 for differing numbers of

prior days (time scales) for 10 species derived from the B4WarmED (Boreal Forest Warming at an Ecotone in Danger experiment) dataset (Reich *et al.*, 2021).

Fig. S18 Seasonal and latitudinal variations of $R_{d,25}$ predicted by H4 with an acclimation time scale of 30 d.

Fig. S19 Temporal changes in global average T_{daily} and T_{night} from 2001 to 2019 and the sensitivities of H1 and H2 to temperature changes.

Fig. S20 Variations of parameter $R_{d,accl}$ used in H2 among 10 species derived from B4WarmED dataset.

Table S1 Information about the field-measured $R_{d,25}$ datasets used in this study.

Please note: Wiley is not responsible for the content or functionality of any Supporting Information supplied by the authors. Any queries (other than missing material) should be directed to the *New Phytologist* Central Office.